Available online at www.sciencedirect.com

ScienceDirect

Procedia Earth and Planetary Science 15 (2015) 619 – 626

Procedia
Earth and Planetary Science

World Multidisciplinary Earth Sciences Symposium, WMESS 2015

Spatial Distribution of Changes in Rockwall Surface at Yoshimi-Hyakuana Cave, Central Japan, Revealed by Repeated Terrestrial Laser Scanning

Yuichi S. Hayakawa[a]*, Chiaki T. Oguchi[b], Natsuki Ariga[c], Hisashi Aoki[c]

[a]*First affiliation, Address, City and Postcode, Country*
[b]*Second affiliation, Address, City and Postcode, Country*

Abstract

For the understanding of weathering processes, quantitative detection and evaluation, including volume estimation, of surficial changes in rocks are fundamental issues. To assess morphological changes in a rockwall, we perform repeated measurement of wall surface using terrestrial laser scanning (TLS) at a test site of Yoshimi-Hyakuana cave in Saitama Prefecture, central Japan. The alignment of time series of point clouds was carried out by tie-point registration method at an initial step, and further refined by cloud-based registration method using the iterative closest point (ICP) algorithm for points on stable surfaces, resulting in registration accuracies of a couple of millimeters. The distances between the point clouds were then computed, and scan errors derived from the laser scanner device itself was found to be at several millimeter scales. Digital elevation models (DEMs) on a vertical plane were then generated from the point clouds, and analyses on the difference raster's of the DEMs successively revealed portions of detachment on the wall surface. The detachment areas have typical depths of 5 to 12 mm and most frequent around 0.6–0.9 m above the ground. Supposed that the detachment is induced by salt weathering, the weathering processes including salt accumulations likely form vulnerable layers at such certain depths on the rock surface. The spatial distribution of the surficial changes will be further assessed by continuous measurements together with monitoring of amount and composition of materials detached from the wall surface.

Peer-review under responsibilty of the Organizing Commitee of WMESS 2015.

Keywords: terrestrial laser scanning; salt weathering; detachment; point cloud; digital elevation model.

* Corresponding author. Tel.: +81471364304.
E-mail address: hayakawa@csis.u-tokyo.ac.jp

Peer-review under responsibilty of the Organizing Commitee of WMESS 2015.
doi:10.1016/j.proeps.2015.08.114

1. Introduction

Among various approaches in weathering studies, the technical development in non-contact, indirect measurements of rock surface morphology using laser scanners has enabled detection and quantitative evaluation of changes in rock surface (Gómez-Pujol et al., 2006; Moses et al., 2014). Such measurements including volume estimation of changes in rock surface are crucial for understanding processes of rock weathering.

Laser scanning approaches have been commonly applied in geomorphological studies in both field and laboratory at various scales. Target objects for laser scanning, often referred to as lidar (light detection and ranging) include desktop-scale objects such as individual gravels where desktop or handheld laser scanners are applied (e.g., Hayakawa and Oguchi, 2005; Bourke, et al., 2008), medium-scale fluvial and hillslope landscapes where terrestrial laser scanners are suitable (e.g., Nagihara et al., 2004; Heritage and Hetherington, 2007; Tarolli, 2014), and large-scale landscapes where airborne laser scanners can cover (e.g., Carter et al., 2001; Sato et al., 2010; Tanaka, 2010; Roering et al., 2013). Among these, small portable laser scanners are often applied as non-contact measurement methods for weathering studies (Moses et al., 2014).

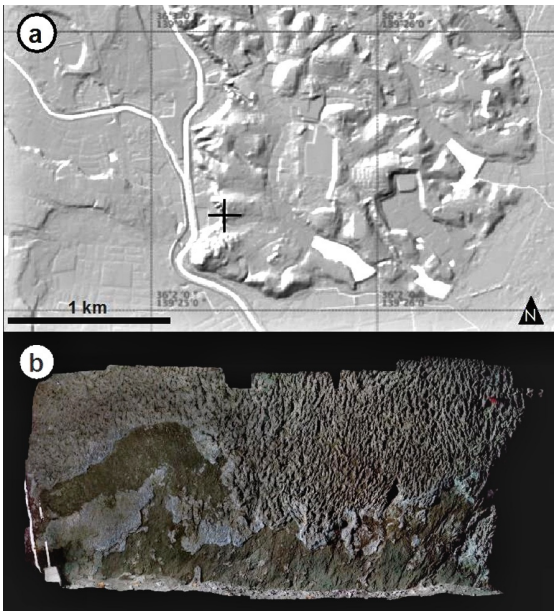

Fig. 1.Study site. (a) Overview of the study area. Cross mark shows the location of Yoshimi-Hyakuana site. Background topographic hillshade image is provided by Geospatial Information Authority of Japan. (b) Orthorectified image of the study plot composed from multiple digital photographs.

Portable laser scanners are applicable to small sample areas (such as ~2,000 cm^2 in area) on flat or gently-sloping outcrops, with accuracies on the order of 0.05–0.1 mm (Swantesson, 1994; Williams et al., 2000; Gómez-Pujol et al., 2006; Meneely et al., 2009). Though lower precision and accuracy, terrestrial laser scanning (TLS) is suitable for measuring wider area of cliffs or outcrops with vertical walls (e.g., Rosser et al., 2005; Buckley et al., 2008), having a capability of analysis on the intensity values of laser returns to detect differences in rock surface conditions (Campos Inocencio et al., 2014). Unlike the traditional point-based measurement of rock surface changes, these relatively new technologies have large advantages in detecting spatial distribution of such subtle changes on rock surface by weathering. However, the accuracies of laser measurement depend on various factors including distance from the scanner to the target surface, laser footprint size, angle of laser pulse and the nature of the surface topography (Schaefer and Inkpen, 2010; Moses et al., 2014). Also, accurate registration of point clouds obtained in different time is crucial for detecting actual volumes or rates of changing surface topography (Olsen et al., 2009; Lague et al., 2013). In order to assess the spatial distribution of surface changes on a rock surface, we perform repeated measurement by TLS at a test plot of an artificial cave wall where salt weathering is actively occurring.

Issues on registration of TLS data obtained in different time are first examined. The actual changes on the wall surface are then extracted, and their spatial distribution is discussed.

2. Methods

2.1. Study Site

The study site is an artificial cave complex named Yoshimi-Hyakuana, located at central Saitama Prefecture in Japan (Fig. 1). The cave complex is formed on the hilly slope of Miocene tuffacious deposits. The site is partly recognized as a cultural heritage composing archaeological stone chambers in tunnel tombs formed in 6-7 centuries AD, while walkable cave complex was formed during the World War II for military reasons. Our test plot is located nearby a west-facing entrance of the cave, where the condition of changing water content due to incoming sunlight and fresh air is favourable for frequent occurrence of salt weathering (Oguchi et al., 2010; Takaya et al., 2011).

2.2. Terrestrial Laser Scanning and Point Cloud Processing

On-site measurements using TLS were performed four times: December 2012 (121213), February 2014 (140225), September 2014 (140922), and December 2014 (141214). One scan position in front of the target wall is set for each time to avoid misalignment of two or more scan positions within one measurement time. For the first measurement (121213), a medium-range terrestrial laser scanner GLS-1500 by Topcon Co. is used (Fig. 2a), which has an ability of measuring 500 m distance at maximum with 1 mm minimum pitch of laser pulse at a rate of up to 30,000 points per second. The weight of the device is 16 kg excluding batteries and other attachments. Initial data management and basic processing of the point cloud data obtained by this device is performed using Topcon ScanMaster v.2.0. For the rest of the measurements (140225, 140922 and 141214), we use a lightweight short-range scanner Trimble TX5 instead of GLS-1500, because TX5 is more suitable for such short range measurements (Fig. 2b). TX5 is capable of measuring up to 120 m in distance at a rate of up to 900,000 points per second. The weight of the instrument is only 5 kg. Trimble RealWorks v.8.1 is used for the initial data processing of point clouds by TX5.

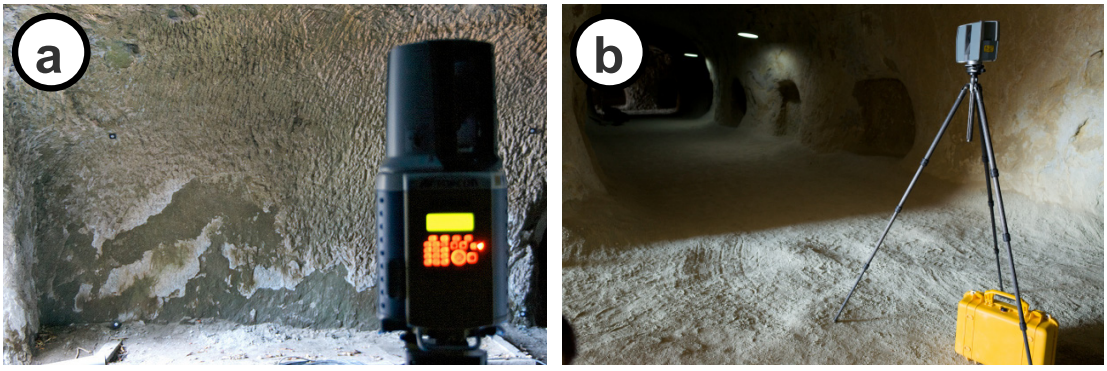

Fig. 2. Terrestrial laser scanners used in this study. (a) Topcon GLS-1500. (b) Trimble TX5.

For comparison of the point cloud data obtained at different times, the point clouds are registered to each other using reference targets installed around the target wall, and the registration is further refined using the iterative closest point (ICP) algorithm (Besl and McKay, 1992; Bergevin et al., 1996) built in the RealWorks software. Such a cloud-based registration method has an advantage in that many tie points (registration targets) are not necessarily installed in such study site recognized as a part of cultural heritage. The first measurement dataset is set as the reference, and each of the following dataset is successively aligned to one previous dataset. The differences in spatial positions between two point clouds are then calculated using the M3C2 (multiscale model-to-model cloud comparison) algorithm functionalized in the open-source software CloudCompare v.2.6.1 (Lague et al., 2013). This algorithm utilizes the normal direction computed within a certain search radius in the original point cloud to obtain the typical distance between the two clouds along the normal direction in the three-dimensional space.

This approach is therefore suitable for direct comparison of three-dimensionally structured point clouds. The periods of comparison are defined as: Period I: 121213 to 140225; Period II: 140225 to 140922; Period III: 140922 to 141214; and Period ALL: 121213 to 141214.

A vertical reference plane is then set based on the reference pins, and the point cloud coordinates were projected on the vertical plane to set the XY coordinates as the location on the wall, while Z coordinate as the change depth of the wall surface. Digital elevation models (DEMs) of the wall surface are then generated from the projected point cloud. Apart from the direct three-dimensional analysis using M3C2, the comparisons using DEMs is limited to one determined direction along the Z axis, but if the target object is flat enough, this approach is suitable because various GIS functions can be applied for the analysis. We use ESRI ArcGIS 10.2 for the DEM data processing. Zones with relatively large changes by detachment are then extracted by vectorising the raster data of differences of the DEMs to which some thresholds are statistically applied.

3. Results

Table 1 shows the properties of point clouds for each measurement series obtained by TLS. The density of the point clouds ranges from 150,000 to 320,000 points per square meters, which are equivalent to average point spacing of approximately 2 mm for each.

Table 1. Properties of point clouds obtained.

date of measurement	Dec. 13, 2012	Feb. 25, 2014	Sep. 22, 2014	Dec. 14, 2014
terrestrial laser scanner used	GLS-1500	TX5	TX5	TX5
number of points	1,596,682	1,068,721	2,301,057	1,722,930
point density (pt/m^2)	222,260.8	149,361.8	323,427.5	238,274.7
average point spacing (mm)	2.1	2.6	1.8	2.0

We installed four steel pins with a size of 2-cm flat head as the reference targets, and the coordinates of the center of pin head were obtained using the target measurement mode in GLS-1500 (accuracy: 0.36 mm) at the first measurement. As noted, this first measurement dataset (121213) was set as the reference, and each of the following dataset was aligned to one previous dataset. The moving dataset was first registered using the reference targets, but the accuracy of the tie-point registration was no better than centimetres likely because of misdetection of the center of the pin heads. The cloud-based, ICP registration was then performed to align two point cloud datasets with higher accuracy. Stable areas without changes on the floor and ceiling of the cave were used for the alignment by cropping out the target wall area, and the ICP registration procedure was repeatedly applied to perform further refinement with minimum error values of the point-to-point distances at 0.6 – 1.7 mm, which seems small enough to detect millimetre to centimetre scale changes in the wall surface (Table 2).

The three-dimensional cloud-to-cloud distances were computed for each Period using the M3C2 algorithm. As shown in the Fig. 3, systematic errors (circular bands of positive and negative difference values) related to the original scan data by the TLS device (TX5) were observed, showing fluctuations around 8 mm. Nevertheless, aside from such errors, some portions in the wall surface show clusters of negative values (blue), which are likely derived from the detachment of the surface material. Such clusters of changes with positive values (red) were also found in part, but they are regarded as not significant because: 1) the lowermost portions of the wall are related to the sedimentation of muddy fragments fallen from the wall, but accurate volumetric estimation of such sediments is difficult because of frequent removal of the sediments by incoming wind; 2) some are related to the presence of spider nets on the wall; and 3) the right-most side of the target area is the corner of the continuous cave wall, and was not properly measured by TLS as the diagonal hit of laser beam resulted in many shadows (lack of laser returns) in the area.

Differences in Z values of the vertically-projected DEMs were computed for each Period within the target domain (Fig. 4). The mean difference of the raster for Period ALL is -1.15 mm, showing net average of recession of the wall surface (Table 2). The zones of detachment changes for each Period were then extracted as follows: According to the mean (up to 1 mm) and standard deviation (up to 2 mm) of the difference raster (Table 2), raster cells with more than 3 mm of detachment were extracted. After generalizing the zones to exclude fragmental cells, the clusters of

cells with detachment changes were vectorised. The volume of detachment for each polygon was then obtained. Because some small fragmental vector polygons still remained, polygons with areas smaller than 0.2 cm^2, equivalent to 5 cells of the 2 mm raster's, as well as those with less than 0.5 cm^3 of volume, were removed. The zones on the lowermost portions, which are the changes of sediments of fallen materials, were also excluded.

Table 2. Properties of difference raster and detachment zones for each period.

properties	data source	Period			
		I	II	III	ALL
duration (month)		14	7	3	24
refinement error (mm)	point cloud	1.7	0.6	0.6	–
mean difference (mm)	difference raster	-1.05	0.12	-0.02	-1.15
standar deviation of difference (mm)	difference raster	1.71	1.13	1.25	1.84
number of detachment zones	polygon	117	15	17	81
mean area of detachment zones (cm^2)	polygon	2.6	3.6	6.0	5.1
standard deviation of area of detachment zones (cm^2)	polygon	2.6	4.2	13.1	12.6
total area of detachment zones (cm^2)	polygon	302.2	53.3	101.7	414.8
mean volume of detachment zones (cm^3)	polygon	1.5	1.9	5.1	3.6
standard deviation of volume of detachment zones (cm^3)	polygon	2.0	2.0	14.3	11.5
total volume of detachment zones (cm^3)	polygon	171.6	28.3	87.3	295.5
mean depth of detachment zones (mm)	polygon	5.4	6.6	7.0	5.9
standard deviation of depth of detachment zones (mm)	polygon	2.2	2.7	3.0	3.0

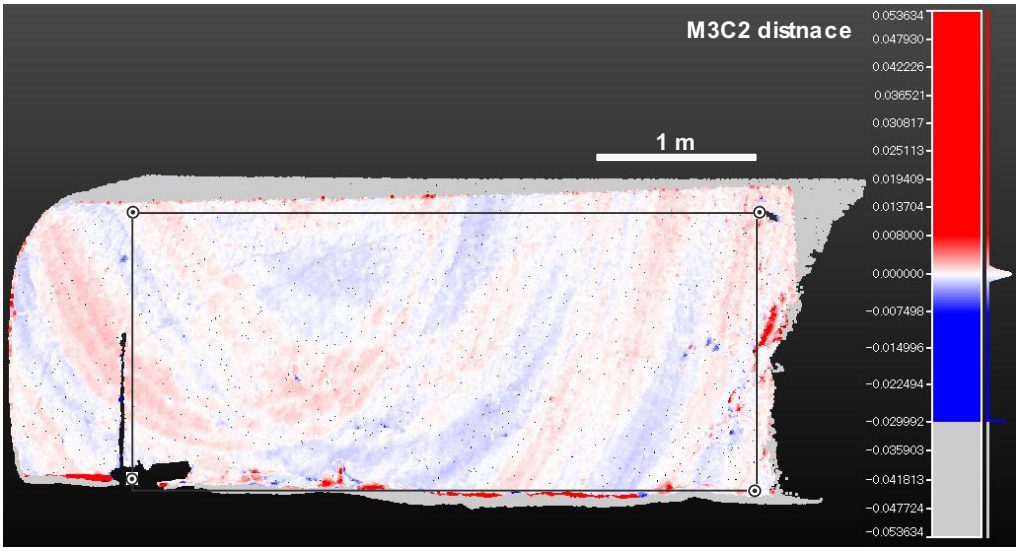

Fig. 3. M3C2 distances between point clouds for Period I (121213 to 140225). Double circles indicate positions of pins, which are used as the target references. Rectangle area shows the target domain for DEM comparisons.

The zone of detachment seems most frequent and largest for Period I (Fig. 4a and Table 2), likely because the duration is the longest (14 months). Despite its short duration (3 months), Period III shows the most distinct zone of detachment (Fig. 4c). This was the largest event of detachment in the wall throughout the study period. Note that the values for Period ALL was derived from the direct comparison between 121213 and 141214, the cumulative values of Periods I to III do not strictly match with those for Period ALL (Table 2). The changes for Period ALL still show the entire trend of the occurrences of detachment on the wall surface throughout the study period.

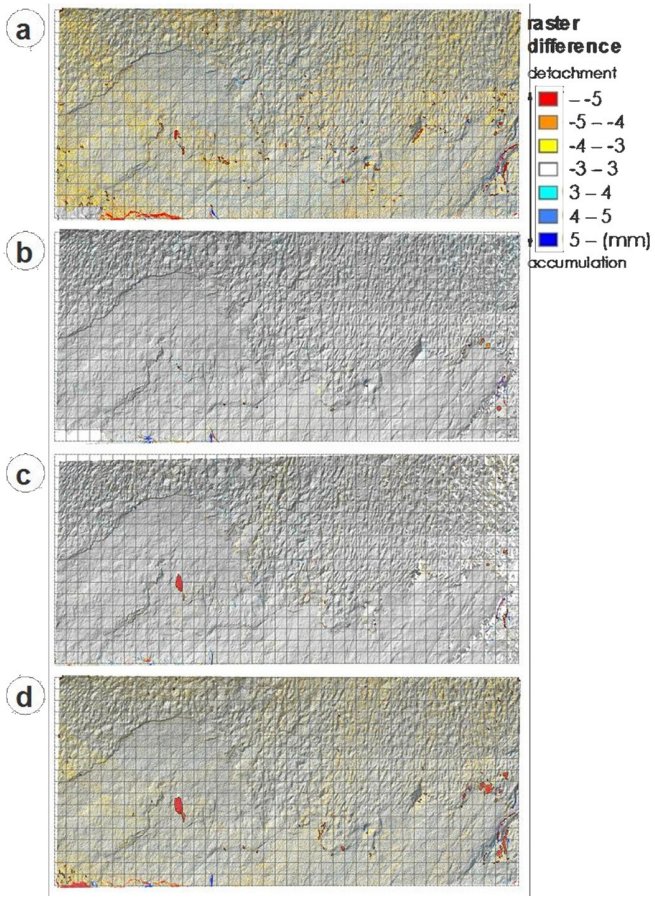

Fig. 4. Differential rasters of DEMs for each Period. Black solid polygons indicate zones with relatively large changes by detachment. (a) Period I (121213 to 140225). (b) Period II (140225 to 140922). (c) Period III (140922 to 141214). (d) Period ALL (121213 to 141214).

The area, volume and mean depth of the detachment zones were then summarized along the y-axis (the height above ground) by a 0.1 m bin. The cumulative volume of changes for the Periods I to III show the largest change at around 0.6–0.9 m high above the ground (Fig. 5a). Whereas, the mean depth of the changes is relatively constant at ca. 5 mm for all the Periods, with some exceptions of ca. 12 mm for Periods II and III.

4. Discussion and conclusions

From the gross difference of the raster for Period ALL (Table 2), the net average rate of the wall surface change (erosion) is estimated to be 0.58 mm/y. This value may indicate the first-order estimate of the weathering rate in this plot, although it does not exceed the error values (>1 mm) and uncertainty remains. For more precise estimate, longer-term measurement will be necessary, as noted later.

The distribution of the detachment zones indicates that the height zone of 0.6–0.9 m above the ground appears to be the central area of frequent occurrences of detachment (Fig. 5a). Supposing that the detachments are derived from salt weathering processes (Oguchi et al., 2010), the height of 0.6–0.9 m appears favourable for the accumulation of salts by frequent evaporation of groundwater, while the groundwater does not seem to reach the higher areas (more than 1.2 m) where the least change is observed.

The mean depth of the detachment of ca. 5 mm (Fig. 5b) may indicate that the frequent detachment is occurring within such thin layer of the rock surface. The occasional depth of ca. 12 mm would be due to the blocky detachment of distinct surface layer of the wall, which can be observed on the wall surface as the clear contrast of

detached and remaining domains (Fig. 1b). Such bimodal distribution of the depth of detachment indicates that weathering is effectively occurring in a certain depth to form vulnerable layers on the rock surface.

Through this study, several challenging issues regarding the TLS approach on the rock surface monitoring would arise. First, the necessity of careful registration for multiple time series of measurement is proposed. In this study, we used the ICP algorithm to perform cloud-based registration of the point clouds at accuracies higher than the tie-point registration. This was because the millimetre-scale accuracy was hard to achieve for detecting center of the heads of the pins having a centimetre width. However, the cloud-based registration is not always perfect giving refinement errors of 0.6–1.7 mm (Table 2) and the manual operation of the cloud-based registration is time consuming.

Second, the surrounding areas of the target wall could not fully be measured due to the presence of shadows for laser returns. Such shadow areas can be reduced if multiple scan positions are set around the target wall. However, the registration issue would also arise for the internal registration of the point clouds from different scan positions for the same measurement time. In fact, we performed measurements from multiple scan positions in the field, but those data were not used because they were found to be unsuitable in such a severe condition for registration of multiple time measurements.

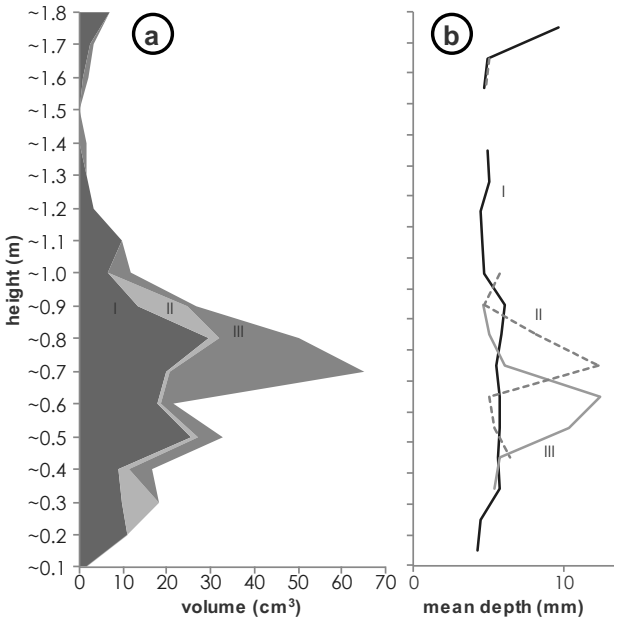

Fig. 5. Distribution of changes in height direction: a) Cumulative changes in volume for each Period (I to III). b) Mean depth of detachment zones for each Period.

Thirdly, the feasible level of detection for the wall surface changes should further be assessed based on the evaluation of errors derived from both registration and scanner itself. In this study, we found that the changes more than ca. 3 mm would be detectable, but the detachments of wall surface by salt weathering can be occurring at much smaller scales (Takaya and Oguchi, 2011; Takaya et al., 2011). To improve the level of detection in the future measurements, further careful operation of the laser scanner, as well as registration process in the software, will be necessary for the reduction of the errors. In addition, further continuous measurements would be required for long-term monitoring and detection of accumulative changes, and comparisons with precise point measurements (e.g., Takaya and Oguchi, 2011) will be performed to verify the amount of detached materials.

Acknowledgement

This study was supported by JSPS KAKENHI Grant Numbers 26350399 and 25702014. This research is a part of CSIS Joint Research No. 587.

References

1. Bergevin, R, Soucy, M., Qagnon, H., Laurendeau, D., 1996. Towards a general multi-view registration technique. IEEE Transactions on Pattern Analysis and Machine Intelligence 18 : 540–547. DOI: 10.1109/34.494643
2. Besl PJ, McKay ND. 1992. A method for registration of 3-D shapes. IEEE Transactions on Pattern Analysis and Machine Intelligence 14 : 239–256. DOI: 10.1109/34.121791
3. Bourke M, Viles H, Nicoli J, Lyew-Ayee P, Ghent R, Holmlund J. 2008. Innovative applications of laser scanning and rapid prototype printing to rock breakdown experiments. Earth Surface Processes and Landforms 33 : 1614–1621. DOI: 10.1002/esp.1631
4. Buckley SJ, Howell JA, Enge HD, Kurz TH. 2008. Terrestrial laser scanning in geology: data acquisition, processing and accuracy considerations. Journal of the Geological Society 165 : 625–638. DOI: 10.1144/0016-76492007-100
5. Campos Inocencio L, Roberto Veronez M, Manoel Wohnrath Tognoli F, de Souza MK, da Silva RM, Gonzaga Jr L, Leonardo Blum Silveira C. 2014. Spectral pattern classification in lidar data for rock identification in outcrops. The Scientific World Journal 2014 : 1–10. DOI: 10.1155/2014/539029
6. Carter W, Shrestha R, Tuell G, Bloomquist D, Sartori M. 2001. Airborne laser swath mapping shines new light on Earth's topography. Eos, Transactions American Geophysical Union 82 : 549–549. DOI: 10.1029/01EO00321
7. Gómez-Pujol L, Fornós JJ, Swantesson JOH. 2006. Rock surface millimetre-scale roughness and weathering of supratidal Mallorcan carbonate coasts (Balearic Islands). Earth Surface Processes and Landforms 31 : 1792–1801. DOI: 10.1002/esp.1379
8. Hayakawa Y, Oguchi T. 2005. Evaluation of gravel sphericity and roundness based on surface-area measurement with a laser scanner. Computers & Geosciences 31 : 735–741. DOI: 10.1016/j.cageo.2005.01.004
9. Heritage G, Hetherington D. 2007. Towards a protocol for laser scanning in fluvial geomorphology. Earth Surface Processes and Landforms 32 : 66–74. DOI: 10.1002/esp.1375
10. Lague D, Brodu N, Leroux J. 2013. Accurate 3D comparison of complex topography with terrestrial laser scanner: Application to the Rangitikei canyon (N-Z). ISPRS Journal of Photogrammetry and Remote Sensing 82: 10–26. DOI: 10.1016/j.isprsjprs.2013.04.009
11. Meneely J, Smith B, Curran J, Ruffell A. 2009. Developing a "Non-destructive scientific toolkit" to monitor monuments and sites.
12. Moses C, Robinson D, Barlow J. 2014. Methods for measuring rock surface weathering and erosion: A critical review. Earth-Science Reviews 135: 141–161. DOI: 10.1016/j.earscirev.2014.04.006 [online] Available from: http://dx.doi.org/10.1016/j.earscirev.2014.04.006
13. Nagihara S, Mulligan KR, Xiong W. 2004. Use of a three-dimensional laser scanner to digitally capture the topography of sand dunes in high spatial resolution. Earth Surface Processes and Landforms 29 : 391–398. DOI: 10.1002/esp.1026
14. Oguchi C, Takaya Y, Ohnishi R, Thidar A, Hatta T. 2010. High acidic sulphate salt production on the cave wall in the Yoshimi Hyaku-Ana historic site, central Japan. 413–419 pp.
15. Olsen MJ, Johnstone E, Driscoll N, Ashford SA, Kuester F. 2009. Terrestrial Laser Scanning of Extended Cliff Sections in Dynamic Environments: Parameter Analysis. Journal of Surveying Engineering 135 : 161–169.
16. Roering JJ, Mackey BH, Marshall J a., Sweeney KE, Deligne NI, Booth AM, Handwerger AL, Cerovski-Darriau C. 2013. "You are HERE": Connecting the dots with airborne lidar for geomorphic fieldwork. Geomorphology 200 : 172–183. DOI: 10.1016/j.geomorph.2013.04.009
17. Rosser NJ, Petley DN, Lim M, Dunning S., Allison RJ. 2005. Terrestrial laser scanning for monitoring the process of hard rock coastal cliff erosion. Quarterly Journal of Engineering Geology and Hydrogeology 38: 363–375. DOI: 10.1144/1470-9236/05-008
18. Sato HP, Iwahashi J, Koarai M, Kamiya I, Komuro K. 2010. Preparation of High-resolution Digital Elevation Models by the Geospatial Information Authority of Japan and Their Applications to Geographic Information Analysis. Transactions, Japanese Geomorphological Union 31 : 359–382.
19. Schaefer M, Inkpen R. 2010. Towards a protocol for laser scanning of rock surfaces. Earth Surface Processes and Landforms 35 : 417–423. DOI: 10.1002/esp.1938
20. Swantesson JOH. 1994. Micro-mapping as a tool for the study of weathered rock surfaces. In Rock weathering and Landform Evolution, Robinson DA and Williams RBG (eds). Wiley; 209–222.
21. Takaya Y, Oguchi CT. 2011. Quantitative evaluation of debris production due to salt weathering of tuff in Yoshimi Hyaku-Ana, an historic site in central Japan. Geographical Review of Japan 84 : 369–376.
22. Takaya Y, Oguchi CT, Yamazaki M, Ohnishi R. 2011. Salt weathering of tuffaceous rock and its influence factor on tunnel walls in the Yoshimi Hyaku-Ana historic site, central Japan. Transactions, Japanese Geomorphological Union 32 : 279–291.
23. Tanaka Y. 2010. Geomorphic Research Using Airborne Laser Swath Mapping and an Introduction to the National Center for Airborne Laser Mapping, U.S.A. Transactions, Japanese Geomorphological Union 31: 345–357.
24. Tarolli P. 2014. High-resolution topography for understanding Earth surface processes: Opportunities and challenges. Geomorphology 216 : 295–312. DOI: 10.1016/j.geomorph.2014.03.008
25. Williams RGB, Swantesson JOH, Robinson DA. 2000. Measuring rates of surface downwearing and mapping microtopography: the use of micro-erosion meters and laser scanners in rock weathering studies. Zeitschrift für Geomorphologie, Supplementbände 120: 51–66.